Four-Scale Linear Model for Anisotropic Reflectance (FLAIR) for Plant Canopies—Part II: Validation and Inversion With CASI, POLDER, and PARABOLA Data at BOREAS

H. Peter White, John R. Miller, and Jing M. Chen

Invited Paper

***Abstract*—To address the need for a flexible model of the bidirectional reflectance distribution function (BRDF) that is also suitable for inversion, the FLAIR Model (Four-Scale Linear Model for AnIsotropic Reflectance) has been developed [1]. Based on the more detailed Four-Scale Model [2], FLAIR is a linear kernel-like model, developed with the aim of not being limited to specific canopy characteristics or view/illumination geometry, while maintaining a direct relationship between canopy architectural properties and model coefficients. Having been previously demonstrated to have the ability to capture the bi-directional patterns in both forward and inverse modes of calculation, this paper examines the FLAIR model in describing the boreal canopy by applying FLAIR to multiangular data sets obtained by various sensors during BOREAS 1994. Effects of sensor field of view, ranges of view/solar illumination geometry, and multiple sensor use on BRDF derivation and inversion for canopy parameter retrieval are considered.**

***Index Terms*—Bidirectional reflectance, mathematical models, model inversion, remote sensing.**

I. Introduction

EFFORTS to monitor global vegetation cover and land surface albedo have lead to extensive investigations of bidirectional reflectance characteristics of vegetative canopies; for example see [3]–[8]. Reviews of these models have also been performed [9]–[10] which help to highlight the benefits and weaknesses of various approaches. As an increasingly detailed influx of data is produced, the need exists for a flexible model of canopy bidirectional reflectance suitable for inversion and that provides quantitative information about canopy architectural and reflectance characteristics that may be used for comparison to other canopies. One such model developed as a result of this is **FLAIR** (**F**our-Scale **L**inear Model of **A**n**i**sotropic **R**eflectance) [1], based on the Four-Scale Model of Chen and Leblanc [2].

The ability of **FLAIR** to model forest canopy reflectance has been demonstrated in part by comparing modeled results to those produced by Four-Scale [1]. Further, when the Four-Scale Model was used to simulate boreal forest canopy BRF data sets (used to validate the Four-Scale Model [2], [6]), inversion with FLAIR provided BRF functions with coefficients that maintained a direct relevance to the canopy characteristics used to produce the simulated data. Application of FLAIR to data obtained from the spaceborne POLDER over Canadian boreal forests has also been demonstrated to provide realistic effective leaf area index, L_e (where $L_e = \Omega \cdot LAI$, the product of the canopy clumping index and the half total leaf area per unit horizontal ground area), and mean overstorey and background reflectance factors [11]. Additional validation and examination of FLAIR with data obtained by airborne CASI, POLDER, and PARABOLA sensors are the subject of this paper.

In short, the FLAIR model is a sum of contributions of four component constituents of the canopy, as described in [1] (and summarized in Appendix A). It is expressed as

$$\text{BRF} = R_{zt} \times k_1 + R_{zg} \times k_2 + R_t \times k_3 + R_g \times k_4 \qquad (1)$$

where R_x are the four scene component mean reflectance factors (zt: shaded overstorey; zg: shaded background; t: sunlit overstorey; g: sunlit background), and k_x are the viewed proportions of the four scene components contributing to the observed BRF, (see Appendix A). These are functions of the view/illumination geometry and the effective leaf area index.

Further, by separating shaded from sunlit contributions, FLAIR provides information on the multiple scattering contribution from both the canopy and diffuse sky. The ratio of shaded to sunlit reflectance factors (as discussed in [1]) is referred to here as the overstorey and understorey multiscattering factors, $C_m F_{dt}$ and $C_m F_{dg}$.

Manuscript received December 4, 2001; revised January 24, 2002. The acquisition of the CASI data, its analysis, and the development of the FLAIR model were supported by an NSERC Operating grant and a Strategic NSERC grant for BOREAS University Investigators to J. R. Miller, York University, Toronto, ON, Canada.

H. P. White is with the Canada Centre for Remote Sensing, Natural Resources Canada, Ottawa, ON K1A 0Y7, Canada (http://www.ccrs.nrcan.gc.ca).

J. R. Miller is with the Department of Physics and Astronomy, York University, Toronto, ON M3J 1P3, Canada (http://www.physics.yorku.ca).

J. M. Chen is with the Department of Geography, University of Toronto, Toronto, ON M5S 3G3, Canada (http://www.geog.utoronto.ca).

Publisher Item Identifier S 0196-2892(02)04815-5.

II. FLAIR Application to Canopy Reflectance

During BOREAS campaigns of 1994 [12], [13] (BOREAS'94), forest canopy reflectance measurements were collected within the northern and southern Canadian taiga biome regions. This was done with a variety of airborne sensors, including POLDER [6], [14], PARABOLA [15], [16], and CASI [17], [18]. The aim is to examine the potential for extrapolation of each derived reflectance function from FLAIR inversion to allow quantitative comparisons between forest sites, and between temporal changes within a site. One aspect inherent within this study is the ability to relate information provided by a variety of remote sensing instruments. Individual sensors each have unique angular and spectral resolutions, and are subject to view/illumination geometry limitations based on sensor location, deployment characteristics, and timing. Thus, each sensor provides a uniquely limited measure of the surface reflectance variations. FLAIR was used to derived inverse functions from BRF observations from each of the three sensors, allowing between-detector and between-site comparisons of the ability to invert measured BRF to obtain a reflectance function and obtain canopy characteristics.

Inversion was performed on each spectral channel individually, with the derived parameters determined by the minimum constraint volume [1]. The minimum constraint volume is derived using a modified simplex method. It is defined as the smallest constraint volume determined by the simplex method that allows all modeled constraints, based on the provided data, to define the bound region within which an optimal feasible vector can pass. This is calculated iteratively for nadir canopy gap fractions, $P_{(i,v)g}(\theta_{(i,v)} = 0°)$, determined as a function of L_e as described in (A6). The value of L_e is iteratively increased, starting at zero, and the FLAIR model inverted to obtain the reflectance factor coefficients at each iteration. This process continues until the minimum constraint volume repeatably increases from one solution to the next. The reflectance factors derived for the value of L_e used to obtain the minimum constraint volume are flagged as the most probable result. For more detail, see [1].

Multiple results (multiple minimum constraint volumes as a function of L_e) occurred in some simulations. In many cases, especially for red spectral bands, these additional results included multiscattering ratios of 0 or 1, with values of L_e less than 0.2 or larger than 5. Two effects were deemed to be responsible here. First, in the red band, BRF values are generally low (<0.05) for boreal canopies. Sensor noise, atmospheric modeling accuracy, and natural variations in surface reflectance may combine to prevent a quantitative measure of canopy BRDF for the range of view/illumination geometry available. In the near infrared (nir), derived reflectance factors and L_e were consistent with measured values from various published studies. At these longer wavelengths, natural variations in surface reflectance and the influence of atmospheric scattering on the remotely sensed signal is less significant relative to the magnitude of the surface reflectance. Derived reflectance factor values will be expected to vary somewhat between sensors and between sensor and "nominal" values as all reflectance factors are determined for differing bandwidths and band centers.

Secondly, multiple scattering characteristics in the overstorey and background levels should be similar in magnitude. Having shaded overstorey receive almost no contribution from canopy multiple scattering and diffuse sky, while shaded background areas receive significant contributions is not realistic, and does not match previous attempts to measure these levels [18], [19]. An additional constraint was thus included to the inversion algorithm, where overstorey and background multiscattering factors are constrained such that the smaller value is within 50% of the larger.

Site biophysical parameters are then determined based on the minimum constraint volume that would simultaneously meet constraints imposed by the infrared BRF data and multiscattering limits, and allow for successful (not optimal) inversion of the visible (red) BRF data. In some cases this minimum constraint volume occurred for a range of L_e. When this happened, the range of results are reported.

A. Applications to POLDER Data

During BOREAS'94, the POLDER sensor was mounted onboard a C-130 airplane and repeatedly flown over each site to obtain multiview angle measures of the canopy reflectance near the principal, perpendicular, and oblique planes, relative to the Sun. Different spectral bands were acquired using a rotating filter wheel in the view path, two are examined here, 670 nm and 864 nm. The sensor was flown at an altitude of 1675 m above ground level (a.g.l.), providing ground pixel dimensions of 35×35 m^2 at nadir. Data was averaged to 3×3 pixels to reduce noise.

Reflectance factors were provided for this study. The 6S atmospheric algorithm [21] was used with a mid-arctic summer atmospheric model, allowing for the derivation of the top-of-canopy reflectance factors from measured top-of-atmosphere radiance values [6]. Reflectance factors derived from July 21, 1994 data, from a 900×900 m^2 area around each site were used. Functions were determined for the forward mode using values recommended by [2] and [6] (Table I), and then by FLAIR inversion to obtain canopy properties (Fig. 1). These data sets provide multiple view angle (multi-θ_v) BRFs for a single solar illumination angle per site (uni-θ_i).

1) Old Black Spruce: Data acquisition occurred with $\theta_i = 33.5°$. Here, the sensor was flown approximately 10° off the solar and cross-solar planes. When applying SSA-OBS nominal site architectural and reflectance factor values (Table I) to produce canopy BRF, it was found that the forward modeled BRF curve reproduced the measured POLDER BRF values. Inversion of this data results in a function that also reproduces these values [Fig. 1(a)]. Note however that the inverse derived reflectance near the horizon starts to increase, resulting in a more "bowl-like" appearance. Canopy parameters determined from inversion suggest a relatively bright overstorey and dark understorey, with a smaller L_e than measured in the field. In the inversion of this uni-θ_i data, the minimum constraint volume ranged between $1.20 < L_e < 2.46$. The upper limit of this range is similar to the value of $L_e = 2.5$ reported by [6]. Within this range, resulting component mean reflectance factors decreased slightly with increasing L_e, also approaching values reported for this site. A summary is provided in Table II.

TABLE I
NOMINAL INPUT MODEL DATA FROM OBSERVED FIELD DATA FOR BOREAS'94 TOWER FLUX SITES

	SSA-OBS	SSA-OJP
Site Location		
Latitude	53.985^0	53.916^0
Longitude	-105.12^0	-104.69^0
Foliage Distribution		
Ω_E *(clumping index)	0.80	0.77
γ_E *(leaf to shoot index)	1.44	1.51
G(θ)	0.5	0.5
LAI (L_e)	4.5 (2.5)	2.2 (1.1)
Reflectance Properties		
R_G (red)	0.04	0.09
C_mF_{dg} (red)	0.05	0.033
R_T (red)	0.11	0.07
C_mF_{dt} (red)	0.027	0.043
R_G (NIR)	0.25	0.17
C_mF_{dg} (NIR)	0.44	0.53
R_T (NIR)	0.50	0.53
C_mF_{dt} (NIR)	0.22	0.25

Adapted from Leblanc et al., 1999. *Adapted from Chen, 1996.

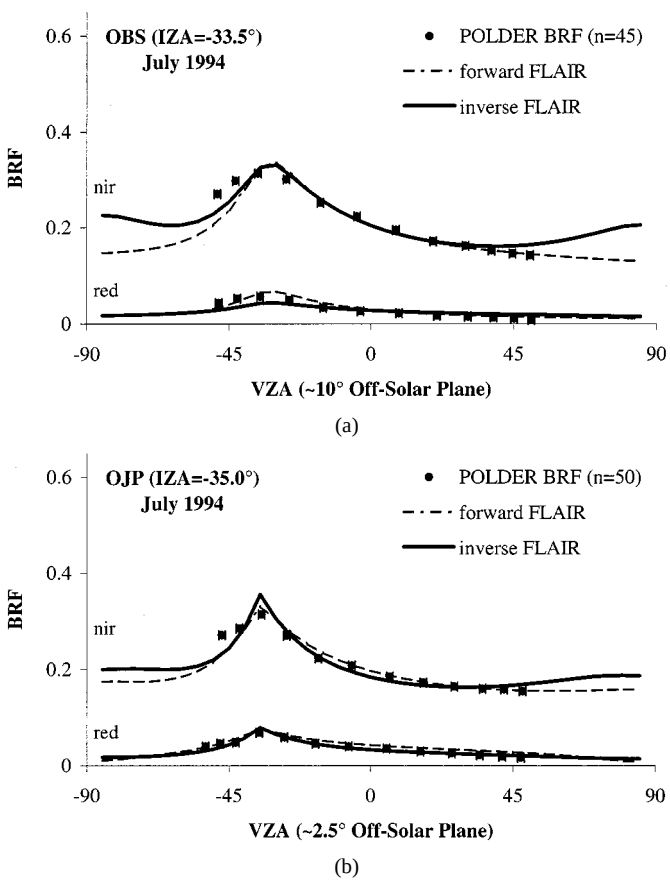

Fig. 1. Near solar plane BRF values for SSA-OBS ($\theta_i = 33.5°$, $\phi \approx$ [10° (backscatter), 170° (forescatter)]) and SSA-OJP ($\theta_i = 35°$, $\phi \approx$ [2.5° (backscatter), 177° (forescatter)]) BOREAS sites as measured by the airborne POLDER. Forward FLAIR results utilize nominal canopy properties (Table I). Inverse FLAIR functions are also shown, using the middle range results as discussed in the text. Horizontal bars indicate sensor field of view.

2) Old Jack Pine: BRF measurements were obtained with $\theta_i = 35°$. Here the sensor was flown closer to the solar and cross-solar planes, within 3°. When applying SSA-OJP nominal site values, it was found that the forward modeled BRF function

TABLE II
CANOPY PROPERTIES DETERMINED FOR THE POLDER SSA-OBS AND SSA-OJP BRF UNI-θ_i DATA SETS BY FLAIR INVERSION. $rmse$ AND r_{cc} VALUES ARE DETERMINED BY COMPARING FLAIR FUNCTIONS TO OBSERVED BRF DATA. PROPERTY VALUE RANGES INDICATE THE RANGE OF THE MINIMUM CONSTRAINT VOLUME DETERMINED DURING THE INVERSION PROCESS. ARROWS INDICATE THESE RANGES FROM LOW → HIGH L_e. N REFERS TO THE NUMBER OF VIEW ANGLES PER BAND USED IN THE INVERSION

POLDER	SSA-OBS (N=23)		SSA-OJP (N=23)	
	Red (670 nm)	NIR (864 nm)	Red (670 nm)	NIR (864 nm)
C_mF_{dt}	0.14 → 0.15	0.24 → 0.27	0.15 → 0.16	0.37 → 0.38
C_mF_{dg}	0.17 ← 0.30	0.15 → 0.50	0.26 → 0.30	0.25 → 0.71
R_t	0.07 → 0.07	0.55 ← 0.68	0.07 ← 0.10	0.42 ← 0.46
R_g	0.03 → 0.06	0.08 ← 0.13	0.04 → 0.11	0.02 ← 0.12
L_e	1.20 → 2.46		1.90 → 3.19	
RMSE	0.011 → 0.015		0.008 → 0.009	
r_{cc}	0.991 ← 0.994		0.995 ← 0.996	

reproduced this data [Fig. 1(b)]. The inverted FLAIR function also reproduced the general shape and magnitude in both the red and near infrared, with a more "bowl-like" forescatter region. Parameters determined from inversion results in a darker overstorey and brighter understorey, with larger L_e than measured in the field. Again, this uni-θ_i data provided a range of results, with $1.90 < L_e < 3.19$ (Table II). In this case, the lower end of the range is more comparable to the value measured in the field ($L_e = 1.1$). Within this range the inverse FLAIR derived reflectance factor values were generally noted to decrease with increasing L_e.

B. Applications to PARABOLA Data

With the PARABOLA sensor [15], [16] three different spectral bands were acquired during BOREAS'94, centered at 662 nm, 864 nm, and 1658 nm. An angular resolution of 15° was used at an altitude of ∼25 m a.g.l. Partial data sets of the SSA-OBS and SSA-OJP site BRFs were provided for this study. Field reflectance values of the canopy components at 1658 nm were not available for this investigation. Comparison between the multi-θ_i data and POLDER uni-θ_i data demonstrate two significant differences. In the forescatter region, a definite bowl shape is present in the PARABOLA data, but not with POLDER. In the backscatter region, the hot spot is less well defined by PARABOLA, often appearing to extend almost to the horizon. This is probably due in part to the increased angular field of view and wider bandwidths.

1) Old Black Spruce: Here, the forward FLAIR modeled BRF (derived with the nominal parameters discussed above) over-estimate observed values in the forescatter region, and underestimate observed backscatter values [see Fig. 2(a) for $\theta_i = 45°$) for all θ_i. The inverse FLAIR functions better match the general shape and magnitude of the observed BRF, providing better correlation to the forescatter bowl feature. The unusually flat and bright backscatter regions recorded by this sensor are not well modeled by FLAIR. Inverse derived L_e is under-estimated, and reflectance factors are similar to field values (Table III).

2) Old Jack Pine: When examining SSA-OJP data, forward FLAIR functions generally reproduce the shape and magnitudes of measured BRF, but underestimate the extent of the forescatter bowl feature. Inverse FLAIR functions better match this feature

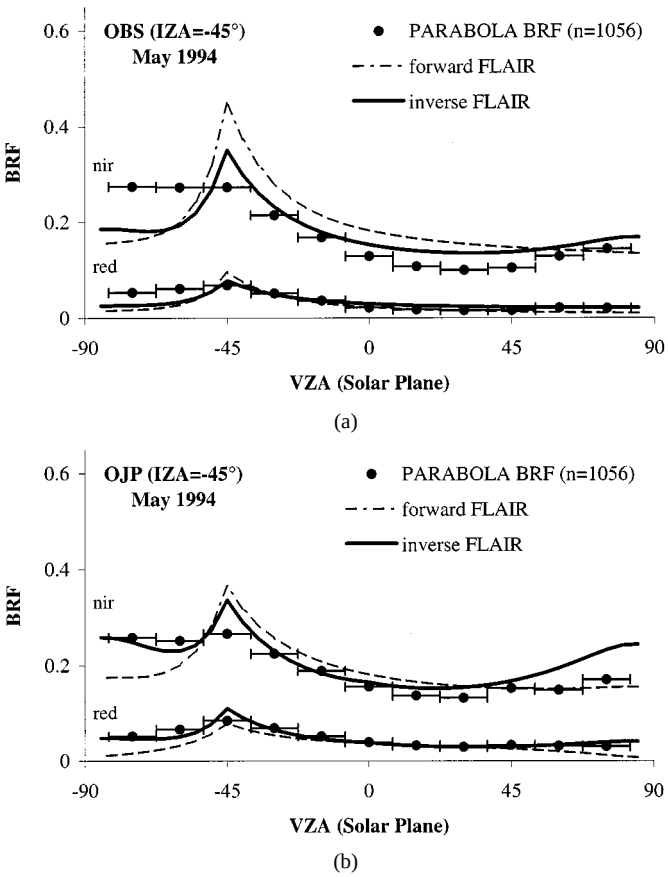

Fig. 2. Solar plane BRF values for SSA-OBS ($\theta_i = 45°$, $\phi \approx$ [0° (backscatter), 180° (forescatter)]) and SSA-OJP ($\theta_i = 45°$, $\phi \approx$ [0° (backscatter), 180° (forescatter)]) BOREAS sites as measured by the PARABOLA. Forward FLAIR results utilize nominal canopy properties (Table I). Inverse derived BRF functions are also shown. Horizontal bars indicate sensor field of view.

[Fig. 2(b)]. Neither function is able to reproduce the measured bright backscatter region. The bright near-horizon BRF determined by the inverse function is due to FLAIR's attempt to fit a low hot spot feature with a bright backscatter plateau. To fit the forescatter region, derived background reflectance factors are decreased (Table III) and multiscattering contributions are increased relative to nominal field observations (Table I).

PARABOLA is subject to relatively coarse spectral (between 60 nm and 200 nm) and angular resolution (15°). This appears to "flatten" the measured BRF around the hot spot, resulting in lower BRF and a hot spot peak which appears more like a hot spot plateau in the $\theta_v > \theta_i$, $\phi \sim 0°$ region. Note how the hot spot peak fits completely within one observational field of view. Also, as PARABOLA operated at a height of ~13 m above the top of canopy (25 m above the ground), the shadow of the instrument may also influence the measured BRF in the hot spot region. At this low height, the ground footprint significantly changes in size, ranging from 9.1 m^2 at nadir to ~80 m^2 at $\theta_v = 60°$, with the average distance to the top of canopy changing from 13 m at nadir to 28 m. Such variations may result in poor sampling of the larger scale tree distribution (50 × 50 m^2) and shadowing effects modeled by FLAIR. The canopy gap probability is no longer a function of a tree groups, but becomes more related to small-scale tree distributions. At nadir the number of crowns viewed may range from a partial crown to as many as 3–4 trees, with up to 11 measurements performed for each view angle. Other observations at 2 m resolution have demonstrated that L_e can easily range ±1 within each BOREAS site [22].

Reported $rmse$ and correlation coefficients (r_{cc}) are calculated using all observed BRFs in the red, NIR, and MIR bands (Table III). With this range of view/illumination geometries, FLAIR inversion was able to converge for both canopies, however the spatial scale of the observations are not adequately modeled by FLAIR, which may explain the poor correlation of derived L_e with field measurements.

C. Applications to BOREAS-CASI Data

BRFs of the SSA-OJP site were obtained from 2 m resolution airborne multi-θ_v imagery taken at 1600 m a.g.l. during February FFC-W and August/September IFC-3 campaigns. The CASI was run in imaging mode, providing two bands for this study. During the winter campaign, bands were centered at 666 nm and 865 nm, with bandwidths of 16 nm and 25 nm, respectively. For the late-summer campaign, bands were centered at 665 nm and 880 nm with bandwidths of 6 nm and 8 nm respectively. Atmospheric correction was performed using the Canadian Advanced Modified 5S (CAM5S) [23]. BRFs were obtained by dividing the 1 × 1 km^2 region centered on the Tower Flux Site into 50 × 50 m^2 sub-sites, with each sub-site averaged to provide a mean BRF comparable to the POLDER data sets discussed above. Each sub-site view orientation (θ_v, ϕ_v) was determined using aircraft GPS and sensor pitch and roll, with θ_i, ϕ_i determined based on time of acquisition and site latitude and longitude [18]. The 16 winter multiangle acquisitions resulted in 5357 BRF values, while the six late summer acquisitions resulted in 1371 BRF values.

Unlike PARABOLA, BRF values taken from CASI spectral imagery have small angular widths (between 0.5° and 3° depending on sensor tilt) and small spectral bandwidths. This smaller spatial averaging does not significantly influence the magnitude and gradient of the BRF curve nearer the hot spot.

As no BRF is obtained at the hot spot during either CASI campaign, the forescatter bowl shape becomes the dominant influence in determining inverse FLAIR functions. Note the relative BRF increase at small scattering angles compared to POLDER and PARABOLA data. At large θ_i, FLAIR kernels indicate that there are significant contributions by shaded components to forescatter BRF [1], while sunlit components are uniquely significant contributors in the hot spot region only. With little BRF observed in this region, model inversion is expected to be less accurate in determining sunlit component reflectance values. Resulting BRF functions are provided in Fig. 3.

1) Summer Old Jack Pine: BRF measurements were obtained with $50° < \theta_i < 68°$. In the forward mode, the derived FLAIR function does not reproduce the magnitude of the BRF near the hot spot [Fig. 3(a)]. The forscatter bowl region however is better defined. This may be due in part to the accuracy of atmospheric correction algorithms at lower sun angles; where multiple scattering becomes more complex,

TABLE III
CANOPY PROPERTIES DETERMINED FOR THE PARABOLA SSA-OBS AND SSA-OJP BRF MULTI-θ_i DATA SETS BY FLAIR INVERSION. $rmse$ AND r_{cc} VALUES ARE DETERMINED BY COMPARING FLAIR FUNCTIONS TO OBSERVED BRF DATA

PARABOLA	SSA-OBS (N=1056)			SSA-OJP (N=1056)		
	Red (662 nm)	NIR (864 nm)	MIR (1658 nm)	Red (662 nm)	NIR (864 nm)	MIR (1658 nm)
C_mF_{dt}	0.15	0.30	0.22	0.20	0.59	0.28
C_mF_{dg}	0.30	0.24	0.26	0.30	0.34	0.42
R_t	0.10	0.49	0.39	0.13	0.32	0.50
R_g	0.03	0.12	0.04	0.03	0.21	0.02
L_e	1.42			1.94		
RMSE	0.056			0.036		
r_{cc}	0.815			0.896		

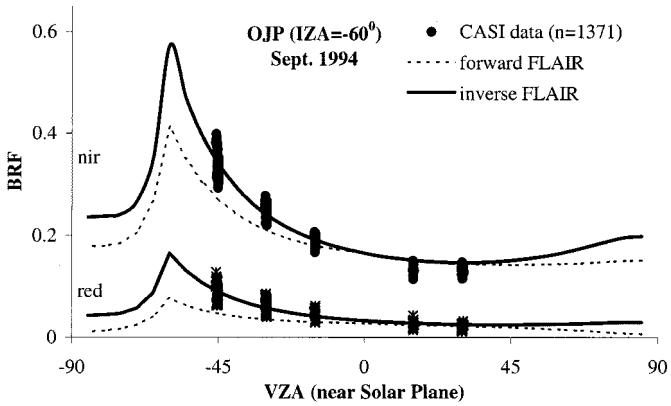

(a)

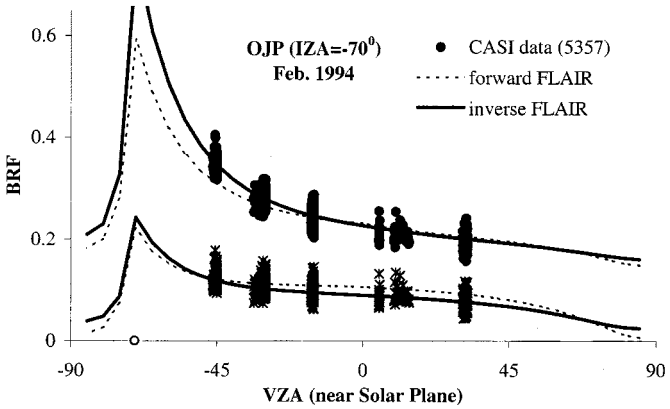

(b)

Fig. 3. Solar plane BRF values for SSA-OJP for late summer ($\theta_i = 60°$, $\phi \approx$ [0° (forescatter)]) and mid-winter ($\theta_i = 70°$, $\phi \approx$ [0° (backscatter), 180° (forescatter)]). BOREAS sites as measured by airborne CASI. Forward FLAIR results utilize nominal canopy properties (Table I). Inverse derived BRF functions are also shown.

and as atmospheric azimuthal asymmetry was not applied. FLAIR inversion derives shaded reflectance factors similar to those determined by inversion for the other cases, with $L_e = 1.30$. Sunlit overstorey reflectance factors however are brighter than those determined with the other data sets, with lower multiscattering ratios (Table IV). This results from the increased gradient in the forescatter hot spot region and lack of data nearer the hot spot and further in the backscatter region.

2) Winter Old Jack Pine: During February, the sun remains near the horizon in Canada, resulting in $69° < \theta_i < 77°$. During this campaign, field measurements of the background snow cover reflectance were performed [18], with a resulting nadir reflectance factor of ~0.85 for both red and nir bands being determined. When this value is used, forward FLAIR functions generally reproduce the CASI BRF winter observations [Fig. 3(b)]. Inversion results in a bright understorey with an overstorey similar in reflectance to the summer inversion, low multiscattering ratios, and $L_e = 1.46$. Winter overstorey reflectance factors and L_e values similar to the summer inversion results demonstrates FLAIR's ability to separate contributions of various canopy components to observed BRF subject to environmentally different conditions.

III. DATA SET COMPARISON

The time scale of the three campaigns provides a temporal baseline ranging from spring to mid-summer to late-summer and winter (for SSA-OJP), with PARABOLA (May 1994), POLDER (July 1994), and CASI (Sept. 1994; Feb. 1994) campaigns. This provides "snap-shots" of canopy BRF throughout one year. Observations of the background [18], [19] and overstorey [6], [25] during the May to September growing period indicate minor changes occurred in the constituents' reflectance. Given this, observed BRF should be similar for each data set, subject only to the BRDF (assuming no sensor and calibration artifacts are present) and the presence of snow in the winter.

Comparisons of inverse FLAIR functions demonstrate similarities between sensors, with POLDER and PARABOLA data inversions resulting in comparable reflectance characteristics and overstorey L_e. However, limiting the data set to one θ_i (POLDER) can prevent FLAIR from converging upon one set of canopy parameters. When multiple θ_i (and θ_v) are used (PARABOLA, CASI) then FLAIR inversion is better able to converge upon a canopy description. This suggests that an increased range of both view and illumination orientations when obtaining canopy BRFs allow for better canopy characterizations, demonstrating the usefulness of multiple angle and multitemporal remote sensing of vegetated surfaces. Comparison between species after inversion of both POLDER and PARABOLA data suggests a slightly larger L_e for the jack pine site relative to black spruce. This is opposite to published field data [6], [25] for these sites. High resolution measurements of overstorey density for these sites [22] suggest that L_e can vary up to ± 1 within a few tens of meters, thus sensor placement may be a contributing factor to this result.

TABLE IV
CANOPY PROPERTIES DETERMINED FOR THE CASI LATE SUMMER AND MID-WINTER SSA-OJP BRF MULTI-θ_i DATA SETS BY FLAIR INVERSION. RMSE AND r_{cc} VALUES ARE DETERMINED BY COMPARING FLAIR FUNCTIONS TO OBSERVED BRF DATA

CASI	FFC-W SSA-OJP (N=5357)		IFC-3 SSA-OJP (N=1371)	
	Red (670 nm)	NIR (864 nm)	Red (670 nm)	NIR (864 nm)
C_mF_{dt}	0.09	0.18	0.09	0.23
C_mF_{dg}	0.10	0.17	0.05	0.30
R_t	0.19	0.75	0.22	0.75
R_g	0.65	0.79	0.02	0.10
L_e	1.46		1.30	
RMSE	0.018		0.025	
r_{cc}	0.865		0.892	

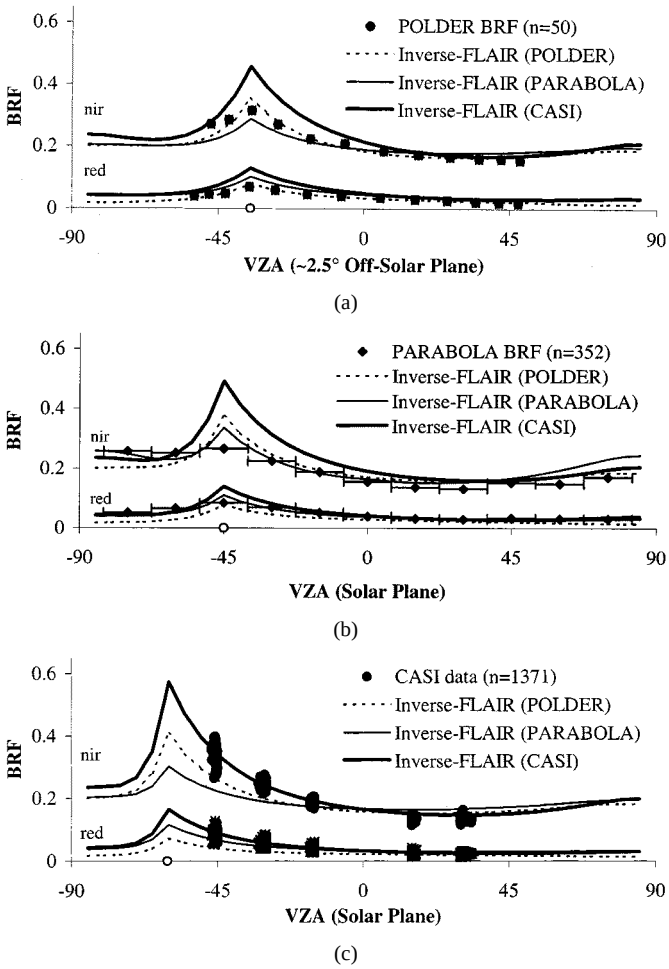

Fig. 4. Solar-plane BRF functions determined by FLAIR inversion using POLDER, PARABOLA, and CASI data sets as discussed in the text.

Direct comparisons of the SSA-OJP canopy parameters derived from inversion have POLDER and PARABOLA data resulting in a denser, darker overstorey relative to CASI inversion results. Quantitative discussion of these values are limited due to the different band centers and widths for each sensor. In all three cases, observed BRFs provide well-defined forescatter regions, with only CASI data not including hot spot or backscatter observations. When using inversion results from one sensor to reproduce data observed at other sensor orientations (Fig. 4), all resulting BRF functions reproduce the forescatter region with differences occurring in the magnitude of the hot spot, related to the model sensitivity in this region to the overstorey density and brightness. With CASI data inversion, overstorey reflectance is determined by the BRF curve gradient in the forescatter region toward the hot spot, and not the backscatter BRF. Also, instrument field of view, band spectral width, and pointing accuracy can influence the measured hot spot and backscatter BRF. As suggested by the FLAIR kernels [1], accurate retrieval of overstorey reflectance and density depends in part on including accurate measurements of the BRFs in these regions.

IV. CONCLUSIONS

In this paper the FLAIR model was examined by inverting boreal forest BRF obtained by three different sensors during different seasonal conditions. Validation of FLAIR has been previously demonstrated with respect to the Four-Scale Model [1] and with space borne POLDER data [11]. As with many other existing linear kernel models, FLAIR has been demonstrated to: i) be able to utilize known canopy architecture characteristics and reflectance to model canopy BRF, and ii) use multiangle reflectance measurements to produce canopy BRF functions applicable to a wide range of solar illumination/view geometries. Unlike these more traditional models however, FLAIR has also demonstrated the potential of iii) determining reasonable and quantitative canopy architectural and reflectance properties through inversion of multiangle BRF measurements. Other models are also being developed with the potential for this capability (such as GHOST [26]), and a comparison between models will help further quantify the ability to use inversion to determine canopy properties.

When the boreal canopy data sets were examined, forward FLAIR functions were able to reproduce measured BRF to a high degree of accuracy (large r_{cc}, low $rmse$) with some discrepancies observed in the hot spot and backscatter region. These discrepancies appear related in part to sensor bandwidth and calibration characteristics, rather than to deficiencies in the FLAIR model.

Inversion provided functions that reproduced measured BRF. In these cases, inverse functions match the magnitude of the hot spot region for each sensor's observations, while maintaining the shape and magnitude of the forescatter region. Comparing results for each sensor individually demonstrates the model's ability to distinguish canopy component characteristics, allowing for monitoring of temporal changes within a site. The potential to compare characteristics between sites is also suggested, but was not sufficiently demonstrated here due to a lack of view/illumination orientations in the data, and in some

cases to small spatial scales. FLAIR demonstrated improved ability to converge upon a canopy parameter set when a range of view/illumination geometry is used. Discrepancies in using FLAIR did appear when inverting reflectance factors observed in the red spectral region. This may demonstrate a sensitivity of FLAIR to natural variations in canopy reflectance not associated with BRDF, or to increased signal-to-noise due to the low signal levels. When inverse functions derived from one data set are used to reproduce BRFs observed by other sensors (at different θ_i) difficulties again arose with the magnitude of the hot spot not being properly reproduced. As this difficulty was not observed when using an individual sensor's data to produce BRF for various θ_i, spatial scale variations as well as sensor band centers and bandwidth and calibration characteristics are believed to be contributing influences.

APPENDIX A

The following is a summary of FLAIR [1]. Symbols are defined in Table V. Canopy BRF may be expressed as

$$R = R_T P_T + R_G P_G + R_{ZT}(1 - P_{vg} - P_T) + R_{ZG}(P_{vg} - P_G). \quad \text{(A1)}$$

After substitution for the probabilities discussed in [1], this may be rewritten into a four coefficient expression in (A2)–(A5), as shown at the bottom of the page, where the proportions of viewed and illuminated background (P_{vg}, P_{ig} respectively) are given by

$$P_{(i,v)g}(\theta_{(i,v)}) = \exp\left(\frac{-G(\theta)\cdot LAI\cdot\Omega}{\cos(\theta_{(i,v)})}\right). \quad \text{(A6)}$$

The probability of viewing within-crown solar-illuminated foliage is expressed as

$$P_{Tf} = \left(1 - \exp\left\{\frac{G(\theta)\cdot\Omega\cdot LAI(S(\theta_i)+S(\theta_v))}{-4\cdot(1-\exp\{-G(\theta)\cdot\Omega\cdot LAI\})}.\right\}\right) \times G(\theta)\cdot\Omega\cdot LAI\left(\frac{S(\theta_i)\cdot S(\theta_v)}{S(\theta_i)+S(\theta_v)}\right) \quad \text{(A7)}$$

(equation updated based on more general description of [27]) where

$$S(\theta_{(i,v)}) = \left(\frac{2\cos(\tan^{-1}(2\tan(\theta_{(i,v)})))}{\cos(\theta_{(i,v)})}\right) \quad \text{(A8)}$$

where a first-order geometric scattering phase function provided by Chen and Leblanc [2] is used here

$$\Gamma(\xi) = \left(1 - \frac{C_p\xi}{\pi}\right), \qquad C_p = 0.75. \quad \text{(A9)}$$

An angular hot spot correlation function is also introduced in [1], as follows:

$$F = \exp\left(\frac{-2\pi\xi}{\xi_{F\max}}\left[1 - \exp\left\{\frac{-G(\theta)\cdot LAI\cdot\Omega}{\cos(\theta_v)}\right\}^{1/2}\right]\right) \quad \text{(A10)}$$

where

$$\xi_{F\max} = \frac{\frac{1}{2}(\pi-\theta_i)\left(1-\left[\frac{\theta_i}{\pi-\theta_i}\right]^2\right)}{1+\frac{\theta_i}{\pi-\theta_i}\cos(\phi_H)} \quad \text{(A11)}$$

$$\phi_H = \tan^{-1}\left(\frac{\theta_v\cdot|\sin(\phi)|}{\theta_v\cdot\cos(\phi)-\theta_i}\right). \quad \text{(A12)}$$

Canopy multiple scattering is expressed as ratios of sunlit to shaded reflectance for the overstorey and understorey

$$\frac{R_{ZT}}{R_T} = C_m\cdot F_{dt} \quad \text{(A13)}$$

$$\frac{R_{ZG}}{R_G} = C_m\cdot F_{dg}. \quad \text{(A14)}$$

ACKNOWLEDGMENT

The authors would like to thank S. Leblanc for his constructive comments, discussions, and assistance in editing that contributed to this paper, and the anonymous reviewers who provided thorough and helpful reviews of this manuscript. They would also like to acknowledge P. Bicheron and M. Leroy for contributing POLDER data and D. Deering for contributing PARABOLA data used in this paper.

REFERENCES

[1] H. P. White, J. R. Miller, and J. M. Chen, "Four-scale linear model for anisotropic reflectance (FLAIR) for plant canopies. I: Model description and partial validation," *IEEE Trans. Geosci. Remote Sensing*, vol. 39, pp. 1072–1083, May 2001.

[2] J. M. Chen and S. G. Leblanc, "A four-scale bidirectional reflectance model based on canopy architecture," *IEEE Trans. Geosci. Remote Sensing*, vol. 35, pp. 1316–1337, May 1997.

[3] W. Wanner, X. Li, and A. H. Strahler, "On the derivation of kernels for kernel-driven models of bidirectional reflectance," *J. Geophys. Res.*, vol. 100, no. D10, pp. 21 077–21 089, 1995.

[4] A. Wu, Z. Li, and J. Cihlar, "Effect of land cover type and greenness on advanced very high resolution radiometer reflectance: Analysis and removal," *J. Geophys. Res.*, vol. 100, no. D10, pp. 9179–9192, 1995.

[5] J. Cihlar, D. Manak, and N. Voisin, "AVHRR bidirectional reflectance effect and compositing," *Remote. Sens. Environ.*, vol. 48, pp. 77–88, 1994.

[6] S. G. Leblanc, P. Bicheron, J. M. Chen, M. Leroy, and J. Cihlar, "Investigation of radiative transfer in boreal forests with an improved 4-scale model and airborne POLDER data," *IEEE Trans. Geosci. Remote Sensing*, vol. 37, pp. 1396–1414, May 1999.

Full Model	Full Model (Kernel Form)	
$R = R_{zt}\times[(1-P_{vg}) - F(1-P_{ig}) - P_{Tf}(1-F)(1-P_{vg})]$	$R = R_{zt}\times k_1$	(A2)
$+R_{zg}\times[P_{vg} - P_{ig}\{F(1-P_{vg})+P_{vg}\}]$	$+R_{zg}\times k_2$	(A3)
$+R_t\times[F(1-P_{ig})+P_{Tf}(1-F)(1-P_{vg})]$	$+R_t\times k_3$	(A4)
$+R_g\times[P_{ig}\{F(1-P_{vg})+P_{vg}\}]$	$+R_g\times k_4$	(A5)

TABLE V
SYMBOL NOMENCLATURE USED IN THIS PAPER

a.g.l.	Altitude above ground level.
BRDF	Bi-directional Reflectance Distribution Function.
BRF	Bi-directional Reflectance Factor.
C_m	Fraction of downwelling irradiance due to multiple scattering within the canopy.
C_p	Foliage asymmetry factor.
F	Hot spot correlation function.
F_{dt}, F_{dg}	Fraction of downwelling irradiance due to diffuse sky irradiance as viewed near the top of the canopy and near the bottom of the canopy respectively.
$\Pi(\xi)$	First-order scattering (geometric shadow) phase function of a foliage element (i.e., needle shoot).
$G(\theta)$	Projection of unit leaf area. ($G(\theta) = 0.5$ is used here.)
ϕ_i	Solar Illumination Azimuth Angle.
θ_i	Solar Illumination Zenith Angle.
k_i	FLAIR kernel designation.
LAI	Leaf Area Index.
L_e	Effective Leaf Area Index ($L_e = \Omega \times LAI$).
Ω	Nonrandomness factor. (Ratio of Ω_E to γ_E).
P_{ig}, P_{vg}	Probability of viewing the understorey.
P_T, P_G	Proportion of sunlit canopy and sunlit understorey respectively.
P_{Tf}	Probability of viewing illuminated foliage when the view and illumination perspectives are not correlated.
P_{ti}	Proportion of observed tree crown that is illuminated.
r_{cc}	Correlation coefficient between modelled reflectance and measured reflectance.
rmse	Root mean square error between modelled reflectance and measured reflectance.
R_G, R_T, R_{ZG}, R_{ZT}	Mean reflectance factor of the sunlit understorey, sunlit crown, shaded understorey, and shaded crown respectively.
ϕ_v	View Azimuth Angle (often given relative to the IAA).
θ_v	View Zenith Angle.
ξ	Angle difference between the Sun and viewer. (scattering angle)
Z_T, Z_G	Proportion of shaded crown and shaded understorey respectively.
ZWH	Zenithal width of the hot spot.

[7] B. Hu, W. Lucht, X. Li, and A. H. Strahler, "Validation of kernel-driven semiempirical models for the surface bidirectional reflectance distribution function of land surfaces," *Remote Sens. Environ.*, vol. 62, pp. 201–214, 1997.

[8] S. Liang, "Narrowband to broadband conversions of land surface albedo. I. Algorithms," *Remote Sens. Environ.*, vol. 76, pp. 213–238, 2001.

[9] N. S. Goel and R. L. Thompson, "A snapshot of canopy reflectance models, and a universal model for radiation regime," *Remote Sens. Rev.*, vol. 18, no. 2–4, pp. 197–226, 2000.

[10] B. Pinty, N. Gobron, J-L. Widlowski, S. A. W. Gerstl, M. M. Verstraete, M. Antunes, C. Bacour, F. Gascon, J-P. Gastellu, N. Goel, S. Jacquemound, P. North, W. Qin, and R. Thompson, "Radiation transfer model intercomparison (RAMI) exercise," *J. Geophys. Res.*, vol. 106, no. D11, pp. 11937–11 956, 2001.

[11] H. P. White, S. G. Leblanc, J. Cihlar, and J. Chen, "Mapping biophysical parameters with modeled and inverted functions from directional satellite measurements," in *Proc. 17th Can. Symp. Remote Sensing*. Quebec, QC, Canada: Laval Univ.

[12] BOREAS, "Boreal Ecosystem Atmosphere Study Experiment Plan Version 3.0," NASA Goddard Space Flight Center, Greenbelt, MD, vol. 4, P. J. Sellers, Ed., 1994.

[13] P. J. Sellers, F. Hall, H. Margolis, B. Kelly, D. Baldocchi, G. den Hartog, J. Cihlar, M. G. Ryan, B. Goodison, P. Crill, K. J. Ranson, D. Lettenmaier, and D. E. Wickland, "The Boreal ecosystem-atmosphere study (BOREAS): An overview and early results from the 1994 field year," *Bull. Amer. Meterol. Soc.*, vol. 76, no. 9, pp. 1549–1577, 1995.

[14] P-Y. Dechamps, F. M. Bréon, M. Leroy, A. Podaire, A. Bricaud, J.-C. Buriez, and G. Sève, "The POLDER mission: Instrumental characteristics and scientific objectives," *IEEE Trans. Geosci. Remote Sensing*, vol. 32, pp. 598–615, May 1994.

[15] D. W. Deering, S. P. Ahmad, T. F. Eck, and B. P. Banerjee, "Temporal attributes of the bi-directional reflectance for three boreal forest canopies," in *Proc. Int. Geosci. Remote Sens. Symp.*, vol. 95, 1995, pp. 1239–1241.

[16] D. W. Deering, T. F. Eck, and B. Banerjee, "Characterization of the reflectance anisotropy of three boreal forest canopies in spring-summer," *Remote Sens. Environ.*, vol. 60, pp. 71–82, 1999.

[17] J. R. Miller, J. Freemantle, P. Shepherd, L. Gray, N. O'Neill, A. Royer, and E. Senese, "Development of CASI to meet the needs of BOREAS science," in *Proc. 17th Can. Symp. Remote Sensing*, Saskatoon, SK, Canada, 1995.

[18] H. P. White, "Investigations of boreal forest bidirectional reflectance factor (BRF)," Ph.D. dissertation, Graduate Programme in Physics and Astronomy, York Univ., Toronto, ON, Canada, 1999.

[19] H. P. White, J. R. Miller, J. M. Chen, and D. R. Peddle, "Seasonal change in mean understorey reflectance for BOREAS sites: Preliminary results," in *Proc. 17th Can. Symp. Remote Sensing*, 1995, pp. 189–194.

[20] J. M. Chen and S. G. Leblanc, "A geometrical multiple scattering scheme to be used in geometric optical models," *IEEE Trans. Geosci. Remote Sensing*, to be published.

[21] E. D. Vermote, J. L. Deuze, and J. J. Morcrette, "Second simulation of the satellite signal in the solar spectrum: An overview," *IEEE Trans. Geosci. Remote Sensing*, vol. 35, pp. 675–686, May 1997.

[22] B. Hu, K. Innanen, and J. Miller, "Retrieval of leaf area index and canopy closure from CASI data over the BOREAS flux tower sites," *Remote Sens. Environ.*, vol. 74, no. 2, pp. 255–274, 2000.

[23] N. T. O'Neill, F. Zagolski, M. Bergeron, A. Royer, J. Miller, and J. Freemantle, "Atmospheric correction of CASI images acquired over the BOREAS southern study area," *Can. J. Remote Sensing*, vol. 23, 1997.

[24] E. M. Middleton, E. A. Walter-Shea, M. A. Mesarch, S. S. Chan, and R. J. Rusin, "Optical properties of canopy elements in black spruce, jack pine, and aspen stands in Saskatchewan, Canada," *Can. J. Remote Sensing*, vol. 23, pp. 188–199, 1996.

[25] J. M. Chen, "Optically-based methods for measuring seasonal variations of leaf area index in boreal conifer stands," *Agric. For. Meteorol.*, vol. 80, pp. 138–163, 1996.

[26] R. Lacaze and J-L. Roujean, "G-function and HOt SpoT (GHOST) reflectance model. Application to multi-scale airborne POLDER measurements," *Remote Sens. Environ.*, 2001.

[27] S. G. Leblanc, P. Bicheron, J. M. Chen, M. Leroy, and J. Cihlar, "Investigation of directional reflectance in boreal forests with an improved four-scale model and airborne PODLER data," *IEEE Trans. Geosci. Remote Sensing*, vol. 37, pp. 1396–1414, May 1999.

H. Peter White received the B.Sc. degree in physics and astronomy from Saint Mary's University, Halifax, NS, Canada, in 1988 and the M.Sc. and Ph.D. degrees in 1994 and 1999, respectively, in physics and astronomy from York University, Toronto, ON, Canada.

He is currently a Research Scientist at Natural Resources Canada, Canadian Centre for Remote Sensing (CCRS), Ottawa, ON. His remote sensing interests have included Jovian planetary atmospheric composition and modeling optical bidirectional reflectance of boreal ecosystems. Current research is focused on applications development of modeling and retrieval of biophysical parameters of vegetative surfaces using optical remote sensing techniques.

John R. Miller received the B.E. degree in physics from the University of Saskatchewan, Saskatoon, SK, Canada, in 1963, and the M.Sc. (1966) and Ph.D. (1969) degrees in space physics from the same university, studying the aurora borealis using rocket-borne radiometers.

He spent two years as a Postdoctoral Fellow at the Herzberg Institute, National Research Council, Ottawa, ON, Canada. In 1971, he joined York University, Toronto, ON, as a Project Scientist. He is currently Professor of Physics and Astronomy at York University and Co-director of the Earth Observations Laboratory of the Centre for Research in Earth and Space Technology (CRESTech). His remote sensing interests include atmospheric correction and interpretation of water color reflectance and canopy reflectance. Over the past decade his primary focus has been on the application of reflectance spectroscopic techniques in remote sensing using imaging spectrometers.

Jing M. Chen received the B.Sc. degree in 1982 from Nanjing Institute of Meteorology, China, and the Ph.D. degree in 1986 from the University of Reading, Reading, U.K.

He is currently a Research Scientist with the Canadian Centre for Remote Sensing (CCRS), Ottawa, ON, and a Professor in the Department of Geography, University of Toronto, Toronto, ON. His main research interests have been in turbulent and radiative transfer processes associated with plant canopies. He is currently engaged in research on applications of optical and microwave remote sensing techniques to boreal ecosystems. Research topics include radiation modeling, biophysical parameter retrieval, and modeling net primary productivity and carbon cycle.